Published in final edited form as:
*Biochim Biophys Acta*. 2009 September ; 1788(9): 1822–1831. doi:10.1016/j.bbamem.2009.06.006.

# Structural and spectropotentiometric analysis of *Blastochloris viridis* heterodimer mutant reaction center

**Nina S. Ponomarenko**[a], **Liang Li**[a], **Antony R. Marino**[a], **Valentina Tereshko**[a], **Agnes Ostafin**[b], **Julia A. Popova**[a], **Edward J. Bylina**[a], **Rustem F. Ismagilov**[a], and **James R. Norris Jr.**[a,*]

[a]Department of Chemistry, University of Chicago, 929 E.57th Street, GCIS, Chicago, IL 60637, USA

[b]Department of Material Science, University of Utah, 316 CME, 122 S. Central Camous Drive, Salt Lake City, UT 84112, USA

## Abstract

Heterodimer mutant reaction centers (RCs) of *Blastochloris viridis* were crystallized using microfluidic technology. In this mutant, a leucine residue replaced the histidine residue which had acted as a fifth ligand to the bacteriochlorophyll (BChl) of the primary electron donor dimer M site (HisM200). With the loss of the histidine-coordinated Mg, one bacteriochlorophyll of the special pair was converted into a bacteriopheophytin (BPhe), and the primary donor became a heterodimer supermolecule. The crystals had dimensions 400×100×100 μm, belonged to space group $P4_32_12$, and were isomorphous to the ones reported earlier for the wild type (WT) strain. The structure was solved to a 2.5 Å resolution limit. Electron-density maps confirmed the replacement of the histidine residue and the absence of Mg. Structural changes in the heterodimer mutant RC relative to the WT included the absence of the water molecule that is typically positioned between the M side of the primary donor and the accessory BChl, a slight shift in the position of amino acids surrounding the site of the mutation, and the rotation of the M194 phenylalanine. The cytochrome subunit was anchored similarly as in the WT and had no detectable changes in its overall position. The highly conserved tyrosine L162, located between the primary donor and the highest potential heme $C_{380}$, revealed only a minor deviation of its hydroxyl group. Concomitantly to modification of the BChl molecule, the redox potential of the heterodimer primary donor increased relative to that of the WT organism (772 mV *vs*. 517 mV). The availability of this heterodimer mutant and its crystal structure provides opportunities for investigating changes in light-induced electron transfer that reflect differences in redox cascades.

### Keywords

*Blastochloris viridis*; Heterodimer mutant; Reaction center structure; Primary donor redox potential; Photosynthetic reaction center; Microfluidic

## 1. Introduction

The photosynthetic reaction center (RC) is a complex of pigments embedded in an integral membrane protein complex that accomplishes light-driven electron transport across a photosynthetic membrane. All components of this photosynthetic core are arranged symmetrically. Two pigment branches extend from the primary electron donor (P), a special



*Corresponding author. Tel.: +1 773 702 7864. jrnorris@uchicago.edu (J.R. Norris)..

pair of bacteriochlorophyll (BChl) molecules, toward a non-heme iron and constitute the two possible electron-transfer pathways. Only one branch, consisting of cofactors associated with the L subunit, is active in electron transfer (ET) while the opposite M side remains non-photoactive. The origin of the asymmetrical charge separation, which starts from the P and continues along only one of the two branches of the RC, can be found in the incomplete sequence homology between the L and M polypeptides along with minor differences in the structural positions of associated prosthetic groups and their corresponding energetic factors [1-4]. Thus, the structure—function relationship between the RC cofactors and the protein moiety defines the unidirectionality of ET that is crucial to fully understanding the process of photosynthesis.

Site-directed mutagenesis has contributed substantially to the investigation of these protein—cofactor interactions. To probe the protein interactions influencing the properties of the primary donor dimer, a series of mutant bacterial organisms has been constructed for spectroscopic and potentiometric examination [5-11]. The properties altered by these mutations have included electrostatic interactions with charged amino acid residues and hydrogen bonding to the conjugated macrocycles or to the Mg of BChl molecules [11]. Alteration of protein coordination to Mg has induced the most significant change in the functional behavior of the RC.

As crystal structures of RCs from purple photosynthetic bacteria *Blastochloris viridis* and *Rhodobacter sphaeroides* have shown, histidines from the L or M polypeptide function as axial ligands to the central Mg atoms of the BChl molecules [3,12]. The substitution of leucine for this histidine residue results in loss of the metal, converting BChl into BPhe and the homodimer P into a primary donor heterodimer (D) [13,14]. Because of the difference in redox potentials of BChl and BPhe [15], this substitution causes substantial changes in the symmetry of the primary donor and in photo-induced ET.

To date, mutations modifying P into a heterodimer have been obtained and investigated only in *R. capsulatus* [16-20] and *R. sphaeroides* [7,21-25]. The production of RC mutants in these species is facilitated by the ability of the WT organisms to express RC pigment—protein complex subunits during non-photosynthetic growth [26,27]. Such aptitude enables both species to produce pigmented, albeit photosynthetically incompetent, subunits of the RC under heterotrophic growth conditions. In addition, the selective pressure of reverse mutations is eliminated, as expressed proteins bearing a mutation are usually nonfunctional.

The ability to alter the RC complex using genetic techniques, the accessibility of optical absorption maxima (located in the near infrared region) for spectroscopic analysis, and the availability of an X-ray structure [12] have all made *R. sphaeroides* a convenient organism for studying structural and functional changes. Despite these advantages, serious limitations for investigation of the re-reduction of the photo-oxidized primary donor ($P^+$) for the next excitation cycle exist because the RC of *R. sphaeroides* does not possess a bound cytochrome subunit. Since the dominant majority of bacterial organisms with photosynthetic ability (excluding cyanobacteria) contains a RC with a bound cytochrome that serves as a direct reductant for the $P^+$, the lack of cytochrome is characteristic of a minority of photosynthetic bacteria [28]. Comparative phylogenetic analyses of photosynthetic microorganisms have suggested that their ancestors possessed this subunit and that its absence is the result of corresponding gene loss in several lines of purple bacteria during the course of evolution [29-31]. Additionally, the basic structure of RC-associated cytochromes is rather uniform, typically containing four hemes [28].

The presence of cytochrome is not just a segregating factor for photosynthetic organisms, but it is also essential in determining the rate of reduction of the oxidized primary donor and thus,

further photochemical charge separation. Without prompt reduction, the $P^+$ state is incompetent for a new photo-excitation event and remains a target for charge recombination with reduced acceptors, leading to a decrease in efficiency of the entire electron-transfer (ET) chain. In *R. sphaeroides*, the measured ET rate includes the effect of docking the soluble cytochrome $c_2$ to the RC and thus depends on the binding affinity of $c_2$ with the RC. Many factors could influence the rate of $P^+$ reduction, including the surface charge of the RC at the site of cytochrome $c_2$ docking [32,33] and a change in the midpoint potential and symmetry of the primary donor caused by the alteration of the surrounding hydrogen bonds [34,35]. Rates of ET in *R. sphaeroides* were found to be approximately proportional to the fraction of spin density on the L side of the special pair ($P_L$) [36]. This suggests preferential ET from the heme to $P_L$. At the same time, structural data for a co-crystal complex of RC and $c_2$ from this organism (along with proposed earlier structural models for the docked cytochrome) presumed major electrostatic interactions and closer contact on the M side of the primary donor ($P_M$) [33,37].

Since the location of the bound cytochrome in *B. viridis* is known from the X-ray structure, uncertainties about docking and binding affinity are eliminated. In addition to the three-dimensional structure and the corresponding *pufC* gene nucleotide sequence, this tetraheme cytochrome subunit has been intensively investigated by various approaches. Optical absorption spectroscopy has been used to determine the peak positions of the individual hemes, and EPR spectroscopy has been applied to reveal their *g*-values [38,39]. Analyses of the redox properties of the individual hemes have shown an alternation of low—high—low—high midpoint potentials in the spatial arrangement of the four hemes in the cytochrome subunit, with the highest potential heme $C_{380}$ (heme 1) located proximally to P [40,41]. The different ET steps from cytochrome have been characterized [42], including restrictions that occur at cryogenic temperatures [43-45]. In addition, the presence of cytochrome, which served as an internal electron donor, was a crucial factor for the determination of the primary acceptor and the intermediate ET carriers at very early stages in the investigation of photosynthesis [46, 47].

All these advantages make *B. viridis* an attractive candidate for investigation of sequential ET and, in particular, beg the question as to what extent the asymmetry of the primary donor plays a role in electron transfer to the primary donor. The most serious constraint for detailed study of the intermolecular ET in this organism has been the difficulty of performing genetic manipulations that impair photosynthetic activity. The typical wild type organism is able to produce the photosynthetic proteins only during autotrophic growth under anaerobic conditions [48]. Introducing a mutation that significantly weakens the photosynthetic functions requires heterotrophic growth of the bacteria, which restricts expression of nonfunctional protein. To eliminate this drawback and to have the possibility to introduce point mutations in the cytochrome subunit, a chimeric RC complex was constructed composed of *B. viridis* cytochrome and core subunits of *Rubrivivax gelatinosus*, the more suitable organism for mutagenesis [49,50]. The primary donor in *R. gelatinosus* had a 100 mV lower redox potential than that of *B. viridis*. This has implications for ET between the *B. viridis* cytochrome and the *R. gelatinosus* RC, as the proximal heme in the *B. viridis* cytochrome would be expected to have essentially the same midpoint potential as the primary donor in *R. gelatinosus*. In the expressed complex the change in potential was more pronounced; the primary donor was found to have an even lower midpoint potential than the WT while the heme had a higher one, indicating a significant alteration in electrostatic interactions [51].

Thus, *B. viridis*, possessing an integrated RC complex whose X-ray structure has been solved to 2 Å resolution [52], is a promising organism to study the reduction of $P^+$ and to address questions about the role of asymmetry in the primary donor. The restrictions on genetic manipulation in *B. viridis* that are due to the inability to produce photosynthetic proteins under

non-photosynthetic growth conditions have been overcome with the development of a genetic procedure based on the heterotrophic strain RA3 [53].

In this paper, we present the structural and spectropotentiometric analysis of the *B. viridis* M side heterodimer mutant His(M200)Leu, constructed using this system. Specific structural details serve as a basis for understanding the altered ET between the photo-oxidized primary donor and its immediate reductant cytochrome.

## 2. Methods

### 2.1. Expression system for B. viridis RCs

Organisms containing mutations affecting the primary donor were constructed via standard protocols [54] employing the RA3 strain of *B. viridis*, which is capable of expressing the photosynthetic apparatus under dark heterotrophic growth conditions [53]. This system uses the chromosomal deletion strain, EYS426, in which the RA3 *puf* operon (carrying genes coding for photosynthetic unit subunits α, β, L, M and cytochrome) has been substituted for a tetracycline interposon by in vitro intron mutagenesis. The deletion begins at the L subunit gene start codon and ends after the cytochrome subunit gene stop codon.

Because the sequence analysis of the *puf* operon and *puh* operon (carrying H subunit codons) in strain RA3 revealed several sequence differences with that of *B. viridis* typical WT strain DSM-133 (ATCC 19567) [1,55], the complementing plasmid containing DSM-133 *puf* structural genes was selected for the construction of the integration vector for the deletion strain. Thus, the resulting organism was designed to contain the L, M and cytochrome subunits of the RC identical to those in the published crystal structure of WT. Since the H subunit had to be inherited from the RA3 strain, it contained two codon differences that result in amino acid substitutions, namely Glu216Asp and Ser256Ala. In addition to the DSM133 *puf* operon, the integration vector (pRL271oriTDSMpufORIKAN1) includes (i) an origin of transfer *oriT*, (ii) a counterselectable *sacB* marker, and (iii) an interposon containing an origin of replication and a kanamycin gene at the end of the *puf* operon. This plasmid was transformed into *E. coli* S17-1 and conjugated into the RA3 *puf* operon deletion strain. The integration of the DSM133 *puf* operon into the EYS426 chromosome produced the strain APW308 containing the *puf* operon from DSM 133 and the *puh* operon (bearing codons for H subunit) from RA3. The RC protein subunits expressed in APW308 are identical to the protein subunits from DSM 133, except for two amino acid substitutions in the H subunit.

### 2.2. Construction of organisms containing mutations affecting the primary donor

Unique restriction sites (non-mutagenic at the amino acid level) were introduced in the DSM133 *puf* operon to facilitate cloning and mutagenesis. Oligonucleotide-directed mutagenesis was used to introduce the restriction sites or to remove doubling throughout the *puf* operon in plasmid pDSMpufORIKAN1. Restriction fragments of this plasmid were subcloned and used as templates for mutagenesis according to protocols described in the ExSite™ PCR-Based Site-Directed Mutagenesis Kit (Stratagene), with some adaptations [53]. After removal of sites BsiWI (~C123), KpnI (~C167); ApaI (~C348), the modifications in the redesigned plasmid pDSMpufORIKAN2 divided the *puf* operon structural genes into smaller regions separated by seven unique and non-mutagenic restriction sites: ApaI, NheI, NsiI, KpnI, BsiWI, BspEI and XbaI. These restriction fragments have been subcloned into pLITMUS vectors to facilitate oligonucleotide-directed mutagenesis experiments on the M and L subunits of the RC, as described below.

Oligonucleotides, which introduced the mutations His M200 to Leu or His L173 to Leu, were cloned into the NsiI—KpnI or ApaI—NheI fragments of the corresponding pLITMUS vectors

using a Stratagene QuikChange Multi Site-Directed Mutagenesis kit. The presence of these mutations was characterized by the appearance of a unique NcoI restriction endonuclease site at ~M200 in the NsiI—KpnI fragment or by the loss of an AflIII site at ~L173 in the ApaI—NheI fragment, respectively (Fig. 1). Each plasmid was recovered by using a QIAgen Spin Miniprep kit and then tested for the presence of the NcoI or AflIII restriction sites. The plasmids were fused with a suicide vector, PRL271oriT, which contained the counterselectable marker *sacB*, conveying sucrose sensitivity (to facilitate isolation of double recombination events). Then the resulting plasmid were transformed into the S17-1 conjugating strain of *Escherichia coli* and conjugated with a rifampicin-resistant RA3 *puf* operon deletion strain, EYS426.

Colonies that had lost the tetracycline resistance contained in the deletion strain interposon and had also gained kanamycin resistance were selected, re-purified, and then tested for the absence of the *sacB* marker. Finally, colonies were examined for the induction of pigmented photosynthetic protein expression under a semi-anaerobic condition in the dark.

### 2.3. RCs isolation, purification and crystallization

Cells with the His(M200)Leu and His(L173)Leu mutations of the primary donor BChl binding site were grown in the dark, under controlled atmosphere (2% $O_2$), pH (6.9) and temperature (30 °C) in a New Brunswick BioFlowIII Fermentation Reactor using RM + PABA medium [56] containing 10 mg/ml kanamycin and rifampicin as described in Bylina et al. [53].

For the isolation and purification of heterodimer mutant RCs, the procedure for preparation of WT RCs [57] was adapted by lowering the concentration of lauryl dimethylamine n-oxide (LDAO) used to solubilize the photosynthetic membranes. At all steps of isolation the purity of the RC was monitored using a Shimadzu 1601 UV—Vis absorption spectrophotometer. For setup of crystallization experiments, the solutions for RCs from the WT were used as previously described [57,58].

RCs were crystallized using plug-based microfluidic technology. Crystallization trials were set up in a polydimethylsiloxane (PDMS) device consisting of four inlet channels (three for the precipitant, buffer, and protein, respectively, and one for the carrier fluid) and one outlet channel. The procedure was the same as previously reported [59]. The precipitant used for the crystallization of the RC from the *R. viridis* heterodimer mutant was 0.15% (w/v) LDAO, 4.0 M $(NH_4)_2SO_4$ in 50 mM $NaH_2PO_4/Na_2HPO_4$ buffer, pH 6.0. The buffer was 0.15% (w/v) LDAO in Millipore water and the RC sample contained 22 mg/ml protein (pH 7.8), 0.08% LDAO, 7% heptane—triol, 4.5% triethylammonium phosphate solution in 20 mM $Na_2HPO_4/NaH_2PO_4$ buffer, pH 6.0. The carrier fluid (FC-40) was a mixture of perfluoro-tri-*n*-butylamine and perfluoro-di-*n*-butylmethylamine. A piece of Teflon tubing, 20 cm in length, with an inner diameter of 500 μm and an outer diameter of 600 μm, was connected to the PDMS device through the outlet channel. To optimize the conditions, the concentration of precipitant was screened between 1.4 M and 1.8 M by varying the relative flow rates of the precipitant and buffer streams using a Labview subroutine. The flow rate of FC-40 was also changed in phase with the precipitant stream to index the concentration by plug size. All the trials, generated in the form of plugs, were transferred into the Teflon tubing, which then was inserted into glass tubing prefilled with perfluorotripentylamine (FC-70). Trials were incubated at 23 °C. The experiment was performed in a low-light environment, and the crystals were stored in the dark.

Crystals were typically 400×100×100 μm at the optimal precipitant concentration of ~1.7 M. These crystals were finally flowed into a well containing a cryo-protectant (2 μl paraffin oil HR3-421, Hampton research), looped with nylon loops (Hampton research), and then stored in liquid nitrogen for X-ray diffraction.

### 2.4. Data collection, refinement and model building

The X-ray diffraction experiments were performed at BioCars 14 BMC of the Advanced Photon Source (Argonne National Laboratory). X-ray data were collected at 100K. Monochromatic radiation with a wavelength of 0.9002 Å was used throughout the data collection with 20 s exposure times and an oscillation width of 0.5°.

The diffraction data from a single crystal was processed with the HKL2000 package [60] to 2.5 Å resolution with a completeness of 99.2%. The crystals belonged to space group $P4_32_12$ with cell dimensions $a=b=220.1$ Å, $c=112.7$ Å and were isomorphous to ones reported earlier with PDB codes 1dxr (2.0 Å resolution) [52] and 2i5n (1.96 Å resolution) [59].

We used the 2i5n structure as a starting model in our refinement. The rigid-body positional and temperature factor refinement was performed using a maximum likelihood target with the program REFMAC5 [61]. The Sigma A-weighted $2F_{obs}—F_{calc}$ and $F_{obs}—F_{calc}$ Fourier maps were calculated using CCP4 [62]. The Fourier maps were displayed and examined in TURBO-FRODO [63]. The search for new solvent molecules was performed with the help of the ARP-WARP program [64]. Water molecules that refined with temperature factors higher than 70 $Å^2$ were discarded from the model. Our model contains 730 water molecules. Figures showing the electron-density map and three-dimensional structures were prepared by using Coot [65].

### 2.5. Spectropotentiometric titration

The oxidation—reduction midpoint potential ($E_m$) of the primary donor was determined spectropotentiometrically by monitoring the absorption spectrum that corresponds to the applied redox potential [66]. Redox titrations were carried out in a 1-cm rectangular optical cell, similar to the one previously described [67], with an electrode assembly connected to a Princeton Applied Research Model 263 potentiostat/galvanostat. Gold mesh, placed at the bottom and the two frosted sides of the cuvette, was used as the working electrode. To promote ET and prevent denaturation of the protein due to adherence, the working electrode was coated by the modifier 4,4′-dithiodipyridine [68]. The auxiliary electrode was a platinum wire. A miniature Ag/AgCl electrode in 3 M KCl (Cypress Systems) was utilized as a reference to which all potentials were referred. To convert values measured with the Ag/AgCl reference electrode to potentials against the standard hydrogen electrode (SHE), +208 mV was added. The potentiostat was calibrated using a fresh standard solution of potassium ferricyanide and potassium ferrocyanide, each at 5 mM, in 0.01 M Tris buffer at pH 8.0 and 25 °C. Under these conditions, the formal potential value for this couple is +0.4084 V *vs*. the SHE [69].

RCs isolated from the deletion strain complemented with the WT genes served as the “reference WT” for the spectropotentiometric titration. This “reference WT” has two amino acid substitutions in the H subunit relative to the standard WT.

Isolated RC complexes were suspended to the final concentration 4–15 mM in 20 mM Tris buffer (pH=7.9) containing 0.05% LDAO, 1 mM EDTA, and 125 mM KCl. Immediately prior to the experiments, the redox potential of the reaction medium (2 ml of RC suspension) was poised with 0.25 mM potassium ferrocyanide and 0.4 mM dicyanobis(1,10-phenanthroline) iron (II) dehydrate. The higher $E_m$ of the last mediator, relative to the potassium ferro-ferricyanide redox system [70], makes it more suitable for mutants with elevated redox potentials of their primary donors [21,71].

At each applied potential, an absorption spectrum was recorded using a Shimadzu 1601 UV—Vis absorption spectrophotometer. Recording did not commence until after equilibrium was achieved, as evidenced by cessation of absorbance changes. The extent of the reduction of the primary donor was determined by measuring the change in optical absorption of the dimer peak (970 nm in the WT, 965 nm in the mutant) as a function of the ambient potential applied. The

midpoint potentials were calculated in Origin by applying the sigmoid fit simulation and verified by fitting the data to the Nernst equation for the one-electron process:

$E=E^{\circ} - \frac{RT}{nF} ln\left(\frac{[\mathrm{Red}]}{\mathrm{Ox}}\right)$ where $E$ is the measured equilibrium potential at each point in the titration, $F$ is the Faraday constant, $E°$ is the formal potential value for the reduction of the RCs and $n$=1.

## 3. Results

### 3.1. General structural features

Comparing the high quality diffraction data collected for the heterodimer mutant RC (2.5 Å resolution) with the excellent quality model of the WT structure (verified at a precision of 1.96 Å [59]) allowed detailed analysis of the spatial modifications of the protein matrix and cofactors. The crystal data, data collection, and refinement statistics are summarized in Table 1, and an example of an electron-density map after completion of all refinements is shown in Fig. 2. Note that the average B-factor of the mutant structure is approximately 1.3 times that of the WT structure for both the protein matrix and the porphyrin cofactors. In those instances where detected changes in the M mutant structure are within or very close to coordinate error, we discuss the trend or direction of deviations.

### 3.2. Structural changes in and around primary donor of M mutant

The electron density around the mutation site and near the primary donor region was well defined. Examination of the corresponding electron-density map (Fig. 2) shows a leucine residue substituting for histidine in position M200, in accordance with the mutation (Fig. 3).

The lack of electron density in the center of the pigment molecule associated with the M subunit confirms the conversion of BChl to BPhe. The overall location of the primary donor porphyrin dimer in the heterodimer mutant did not appear to be changed significantly relative to the WT, but the distance between the centers of macrocycles slightly decreased to 7.4 Å (7.64 Å in the WT). In the structure of the primary donor, the orientation of the tetrapyrrole rings relative to each other has two minor modifications relative to the WT. First, the BPhe molecule is slightly bent toward the BChl counterpart with 8° of rotation modifying the angle between the overlapping rings (Figs. 2 and 4). Second, there is a small shift of the rings A and B of the BChl molecule toward the BPhe moiety, with corresponding acetyl and etylidene substitution displacements of 0.4 and 0.5 Å, respectively. As a result of such opposite moves, the interval between the overlapping rings of the conjugated porphyrin macrocycles diminished to 3.1 Å from 3.4 Å in the WT. In the heterodimer mutant RC, the L side of the porphyrin dimer appears to be slightly pushed by the histidine ligand toward the BPhe[AU1]. The Mg-sustaining HisL173 also moved 0.43 Å in the same direction as the BChl counterpart of the porphyrin dimer. Owing to this conjugate shift, the interval from HisL173 to the remaining Mg atom persisted at 2.1 Å, equal to the His NE2—Mg distance in the WT.

Although deviations in the structures of the macrocycles appear to be relatively minor in the heterodimer mutant primary donor, the analysis of electron-density map revealed that the BPhe ($D_M$) molecule is more disordered than its BChl ($D_L$) counterpart. This differentiation is more significant for the macrocycles themselves than for the phytyl tails of the two pigments, with the mean B-factor for the BChl equal to 26.5 *vs*. 40.4 for BPhe. The WT RC has almost equivalent B-factors for the constituent $P_L$ and $P_M$ components, 15.4 and 16.4 respectively. Notably, the phytyl tail of BPhe molecule was modeled in a slightly different configuration than the BChl counterpart. This is in contrast to the WT, where the pseudo two-fold symmetry of the porphyrin dimer heterocycles corresponds to the structure of the phytyl chains also. Besides, as was shown by a comparison study of RCs crystal structures, the phytyl chains of the *B. viridis* special pair have a similar fold to that in several *R. sphaeroides* structures [72].

Considering the thermal factors together with the modified folding, we assume that an increase in mobility of the phytyl chain occurs in the BPhe counterpart of the heterodimer primary donor.

Minor structural modifications of the protein core around the BPhe molecule were also detected. In the region between the M194 and M206 amino acids that surround the site of mutation, the most significant shift in the peptide backbone was 0.6 Å for TrpM199 toward the BPhe molecule. Spatial alterations for corresponding amino acid side chains followed the same direction. Isoleucine 204, spatially the closest amino acid to the overlapping A rings, was relocated 0.56 Å away from M200 and toward the BPhe counterpart without changes in the orientation of its side chain.

The distance between the TyrM195 and the acetyl carbonyl oxygen of the A ring of $D_M$ (BPhe), which are joined by a hydrogen bond, decreased to 2.2 Å from 2.8 Å in the WT. The interval for the symmetry-related hydrogen bond between HisL168 and the ring A acetyl carbonyl group of $D_L$ increased to 3.0 Å from 2.8 Å in the WT. The other hydrogen bond forming amino acid, ThrL248, moved 0.28 Å toward $D_L$, but the length of the hydrogen bond remained 2.65 Å because of the simultaneous movement of the BChl molecule. The amino acid neighboring ring C of $D_M$, PheM194, was rotated 28° (Fig. 4). This was the most significant change of position for an amino acid in the vicinity of the primary donor.

The other major difference in the structure of the heterodimer mutant RC from that of the WT was the absence of a water molecule located 2.9 Å from the M200 histidine (Fig. 4). Normally this water molecule creates hydrogen bonding among the histidine imidazole side chain, the keto substituent of the E ring of the L side accessory BChl, and the backbone carbonyl oxygen atoms of Tyr M195 [3].

In response to the absence of hydrogen bonding, the adjoining rings of the accessory BChl shifted in the direction of the cavity filled by water in the WT RCs. The most noticeable displacement occurred to the keto carbonyl oxygen atom formerly involved in that bonding (0.53 Å). Concomitantly, the side chain of TyrM195 moved toward $D_B$ (primary donor BPhe), as described before. A water molecule in an analogous position is found between HisL173 and the accessory BChl of M side similar to the WT structure.

### 3.3. Structural changes in cytochrome subunit

No significant structural modifications of the protein matrix around the hemes of the cytochrome subunits were detected. For both structures, electron density was continuous for the entire backbone and the density representing the four bound porphyrin heme groups was clearly defined. All side chains were modeled, including solvent-exposed residues. The positions of the heme 4, distal to the primary donor, are almost identical in the WT and in heterodimer mutant RCs. There were some local conformational differences in the vicinity of the iron atoms in the rest of the hemes. Changes in positions of the corresponding ligands of the protein matrix are very small and stay within coordinate error (0.215 Å). The shift of histidine C248, which is a ligand of heme 1, amounted to 0.03 Å, whereas MetC233 remained in the same place. For both histidine ligands of heme 2, displacements did not exceed 0.02 Å. At the same time, the angles between the bonds created by coordinating Fe ligands decreased by 3.3, 7.3, 9.2, 1.4° for hemes 1–4, respectively. The deflection of ligand bonds, almost perpendicular to the plane of the hemes in the WT, is most notable for the mutant's heme 3. No changes in positions of the amino acids ArgC 202, 264, 272 and AspM314, those involved in tuning of the electrochemical potential of heme 1, were detected, and there were no discernable modifications in the arrangement or coordination of the amino acids influencing the redox properties of hemes 2–4.

For the highly conserved tyrosine L162, located between the proximal heme 1 and P, the displacement of the hydroxyl group was found to be 0.35 Å.

### 3.4. Structural differences in H subunit

The construction of organisms containing mutations affecting the primary donor required conjugating DSM-133 *puf* structural genes with the rest of the RA3 strain genome of *B. viridis*. For this reason, the resulting heterodimer mutant RCs consisted of L, M and cytochrome subunits from the WT *B. viridis* (PDB codes 1prc or 2i5n) and the H subunit from the RA3 strain, which has two amino acid substitutions relative to the WT. Both alterations, Glu216Asp and Ser256Ala, were detected in the structure of the M-heterodimer mutant. The first mutation, the replacement of glutamate with chemically similar aspartate, influenced only the length of the side chain and did not change the reactive groups. The second mutation, the replacement of serine with alanine, shortened the side chain, removed the highly reactive hydroxyl group, and converted the amino acid from polar to hydrophobic. Both mutations were located on the surface of the H subunit, away from the primary donor, and were assumed to have no influence on its properties.

### 3.5. Spectropotentiometric titration

The comparison of electrochemical titration curves corresponding to the primary electron donor of the M mutant and WT strains, represented in Fig. 5, revealed the increase of redox midpoint potential in the modified organism. The titration curve in the WT could be satisfactorily fitted with a Nernst curve with $E_m$=516.9±5.3 mV, in agreement with previous measurements [51,73,74]. The reverse titration was possible only for the WT RCs. Because of the elevated potential of the heterodimer primary donor, $E_m$=772.0±11.4, the RCs were insufficiently stable to conduct a reverse titration after oxidative titration. Additionally, the high potentials resulted in greater variability among measurements of the midpoint potential in the M mutant. Nevertheless, the measurements were reproducible to within about 25 meV.

## 4. Discussion

The diffraction data indicated that the mutation introduced in the primary donor environment caused no significant changes to the overall tertiary protein structure, including that of the cytochrome subunit. A few differences between the two structures were evident around the mutation site. The major observable structural changes were in accordance with the expectations of the mutation. In the absence of a coordinating ligand for the Mg atom, BChl was replaced by BPhe. The water molecule involved in the hydrogen bonding of histidine and the L side accessory BChl was missing. The absence of the water molecule in the analogous position was also found in the previously reported structure of the *R. sphaeroides* heterodimer mutant RC [25]. Concomitant to water disappearance was the shift of the amino acids surrounding the mutation site up to 0.6 Å and the rotation of PheM194. The amino acid closest to the missing water molecule, the conserved isoleucine M204, was one of the most shifted moieties, deviating 0.56 Å from M200 toward ring A of the BPhe molecule. Because we did not detect rotation of this isoleucine residue into the cavity where the missing water would be, as was detected for the M-heterodimer mutant of *R. sphaeroides* [25], we suggest that the disappearance of the water molecule was the direct consequence of the replacement of histidine by leucine. The existence of analogous structural changes in the heterodimer mutants of *B. viridis* and *R. sphaeroides* allows us to presume that this specific water loss accompanies the mutation and the positional adjustment of the amino acids is the secondary or following event.

Due to the loss of this water molecule, the hydrogen bond to the accessory BChl vanished; this should result in the alteration of its midpoint potential. As was demonstrated in experiments with *R. sphaeroides*, the presence of hydrogen bonds to the conjugated macrocycle of

porphyrins is one of the major factors that modulate the primary donor midpoint potential [11,21]. Because removal of the hydrogen bond to the carbonyl group usually leads to a decrease of the midpoint potential of the corresponding pigment [11], we can expect an analogous decrease of this parameter for the accessory BChl. This reduction in the midpoint potential should make the accessory BChl a less efficient reductant and consequently alter the related functions of this cofactor. Analysis of the spectroscopic data of *R. sphaeroides* heterodimer mutants indeed detected the existence of perturbations in the electronic structure of accessory BChl, complementary to the altered electronic properties of the modified primary donor [18,22,75].

Shortening of the hydrogen bond to $D_M$ and elongation of the hydrogen bond to $D_L$ reflect structural adjustment to the modified position of the primary donor and also can impact its redox properties. The influence of these contra-directional alterations on the midpoint potential of the primary donor is, however, expected to be minor, especially compared to the change in electrochemical potential caused by its conversion to a heterodimer.

### 4.1. Rotation of phenylalanine 194 of M subunit

The observed rotation of PheM194 in the mutant points to its possible interaction with the histidine M200 and suggests potential roles of histidines in the WT RC. Besides the significance for enzymatic catalysis, histidine is one of the most important amino acids in the context of protein tertiary structure. In addition to its major role in determining porphyrin metal ligation, this amino acid is also involved in protein-stabilizing interactions [76,77], particularly those in the hydrophobic cores of protein. The importance of interactions between the imidazole ring of histidine and the aromatic ring of Tyr, Phe or Trp has been estimated in protein engineering and modeling experiments. As a result of the extensive analysis of aromatic amino acid coordination performed on the structures deposited in PDB, histidine has been classified as a highly interacting aromatic residue [78,79]. In that study, the aromatic amino acid pairs were defined based on spatial proximity, with a requirement of less than 5.5 Å distance between side chains [80]. In the WT RC structure of *B. viridis*, the distance from HisM200 to PheM194 amounts to 4.48 Å, pointing to the possible existence of an aromatic pair. This also indicated that detected rotation of phenylalanine in the heterodimer mutant was most probably the result of the loss of the hydrophobic interaction with HisM200 rather than just the disappearance of steric hindrance.

A study on amino acid interactions and protein stability found histidine, along with other aromatic amino acids, to act as a strong hub [81], usually involved in multiple interactions within the protein. In contrast the hydrophobic leucine usually forms a weak hub. Because they bring together different elements in the tertiary structure of a protein, amino acids forming hubs are crucial for the unique three-dimensional structure of proteins. We can speculate that by replacing the histidine with leucine, the highly interacting hub was converted to a significantly weaker hub, influencing the protein matrix stability. Although the mutation did not cause significant reorganization of the protein matrix, it has the potential for increasing the conformational flexibility of the protein macromolecule.

### 4.2. Displacement of tyrosine 162 of L subunit

We also detected a 0.35 Å displacement toward the primary donor of the hydroxyl group of tyrosine L162, located between the primary donor and the proximal heme group (heme 1) of the cytochrome. This highly conserved tyrosine residue was found at the same position in all RCs sequenced for photosynthetic bacteria. In the three-dimensional structure of the *B. viridis* RC, it is positioned halfway between the P and the heme 1 [3,82]. This attribute led to the assumption that this tyrosine residue plays a critical role in the cytochrome-mediated reduction of the photo-oxidized BChl dimer [83,84]. In attempts to understand its function,

this tyrosine has been replaced by other amino acids through site-directed mutagenesis in *B. viridis* [45,73,85] and in *R. sphaeroides* [32,86,87]. These analyses established the role of this residue as mainly structural. The presence of this tyrosine residue ensures that the cytochrome subunit is properly aligned with the RC in organisms with a permanently bound electron carrier, represented by *B. viridis*, or supports an ideal docking site for the soluble cytochrome $c_2$ (the direct reductant for oxidized primary donor) in organisms such as *R. sphaeroides* [88]. This tyrosine residue has also been shown to be involved in a network of hydrogen bonds with the heme-ligating histidine C248 and tyrosine M195 (hydrogen-bridged to P). How much this network was modified with the concomitant shift of the tyrosines at positions M162 and M195 is beyond the scope of this paper such that we can only speculate. Certainly, this small structural alteration taken alone cannot significantly influence the reduction of D by the cytochrome but might amplify changes introduced by the increase in redox potential of the primary donor.

### 4.3 Spectropotentiometric titration

The midpoint potential determined for the primary donor of *B. viridis* heterodimer mutant is higher than the 640–658 mV previously reported for the analogous *R. sphaeroides* mutant [21,89]. The more significant increase in potential might be explained by the greater asymmetry of the primary donor in this organism relative to that in *R. sphaeroides*, as *B. viridis* has the additional hydrogen bonds from TyrM195 to the $P_M$ and from HisL168 and ThrL248 to $P_L$ [3]. An additional hydrogen bond raises the redox potential by stabilizing the neutral primary donor and increasing the energy required to remove an electron from the highest occupied molecular orbital. This orbital has a higher contribution from the $P_L$ constituent relative to the $P_M$ constituent of the primary donor [35]. The Hückel molecular orbital model provides a quantitative relation for interdependence of the midpoint potential and spin density localization of P (or the ratio $P_L/P_M$), which, besides parameters such as the coupling of two molecules ($\beta$), includes the energetic inequivalence ($\Delta\alpha$) of constituents in the conjugated macrocycle. The last parameter is determined by the protein matrix, which provides hydrogen bonds [90-92].

Experiments on mutants of *R. sphaeroides* have shown that the energetics of the excited primary donor and the redox potential of $P/P^+$ can be modified by altering the number of hydrogen bonds to the conjugated macrocycle or the chemical nature of the H-bond-donating amino acid residue [6,11]. Changes in the interaction of the protein matrix and the $P_L$ had a larger effect on the midpoint potential of P than did changes in the interaction of the protein matrix with $P_M$ [5,93]. In the heterodimer mutants, the asymmetry of the primary donor is enhanced by the energetic difference of its counterparts, but the L side remains more sensitive to the introduction of additional hydrogen bonds. In double mutants, where the hydrogen bond alteration complemented the heterodimer mutation, extra hydrogen bonds to the BChl increased the midpoint potential more significantly than those to the BPhe counterpart of the heterodimer [21,94]. Thus, the detected rise in potential of the heterodimer primary donor in *B. viridis* can be explained by the enhanced asymmetry of the primary donor relative to *R. sphaeroides*, an asymmetry caused by an additional hydrogen bond directly to the $D_L$, the more susceptible counterpart of the heterodimer.

## 5. Conclusions

Structural analysis has shown that a mutation affecting the primary donor, in which histidine was replaced by leucine in the M subunit, caused the expected incorporation of BPhe instead of BChl, converting the primary donor into a heterodimer. Minor spatial reorganization of the conjugated macrocycles and the surrounding amino acids revealed the adjustment of the protein environment to the mutation. The concomitant increase in redox potential suggests alterations in the excited state energy and in the re-reduction process of the oxidized heterodimer primary

donor. The availability of this heterodimer mutant from *B. viridis* and its crystal structure provides opportunities for electronic structure analysis of highly asymmetrical primary donors and allows for the investigation of light-induced ET changes that reflect the difference in redox cascades.

## Acknowledgements

We gratefully acknowledge support from the US Department of Energy, Office of Basic Energy Sciences, and Division of Chemical Sciences Contract DEFG02-96ER14675. This work was supported in part through the NIH Roadmap for Medical Research (R01 GM075827-01). We thank Elizabeth B. Haney for contributions to editing this manuscript. L.L and R.F.I. are responsible for the microfluidic crystallization.

## References

[1]. Michel H, Weyer KA, Gruenberg H, Dunger I, Oesterhelt D, Lottspeich F. The “light” and “medium” subunits of the photosynthetic reaction centre from *Rhodopseudomonas viridis*: isolation of the genes, nucleotide and amino acid sequence. EMBO J 1986;5:1149–1158. [PubMed: 15966102]

[2]. Komiya H, Yeates TO, Rees DC, Allen JP, Feher G. Structure of the reaction center from *Rhodobacter sphaeroides* R-26 and 2.4.1: 6. Symmetry relations and sequence comparisons between different species. Proc. Natl. Acad. Sci. U. S. A 1988;85:9012–9016. [PubMed: 3057498]

[3]. Deisenhofer J, Epp O, Sinning I, Michel H. Crystallographic refinement at 2.3 Å resolution and refined model of the photosynthetic reaction centre from *Rhodopseudomonas viridis*. J. Mol. Biol 1995;246:429–457. [PubMed: 7877166]

[4]. Steffen MA, Lao K, Boxer SG. Dielectric asymmetry in the photosynthetic reaction center. Science 1994;294:810–816. [PubMed: 17794722]

[5]. Artz K, Williams JC, Allen JP, Lendzian F, Rautter J, Lubitz W. Relationship between the oxidation potential and electron spin density of the primary electron donor in reaction centers from *Rhodobacter sphaeroides*. Proc. Natl. Acad. Sci. U. S. A 1997;94:13582–13587. [PubMed: 9391069]

[6]. Ivancich A, Artz K, Williams JC, Allen JP, Mattioli TA. Effects of hydrogen bonds on the redox potential and electronic structure of the bacterial primary electron donor. Biochemistry 1998;37:11812–11820. [PubMed: 9718304]

[7]. Nabedryk E, Breton J, Williams JC, Allen JP, Kuhn M, Lubitz W. FTIR characterization of the primary electron donor in double mutants combining the heterodimer HL(M202) with the LH (L131), HF(L168), FH(M197), or LH (M160) mutations. Spectrochim. Acta, Part A 1998;54:1219–1230.

[8]. Mattioli TA, Lin X, Allen JP, Williams JC. Correlation between multiple hydrogen bonding and alteration of the oxidation potential of the bacteriochlorophyll dimer of reaction centers from *Rhodobacter sphaeroides*. Biochemistry 1995;34:6142–6152. [PubMed: 7742318]

[9]. Moore LJ, Zhou H, B. SG. Excited-state electronic asymmetry of the special pair in photosynthetic reaction center mutants: absorption and stark spectroscopy. Biochemistry 1999;38:11949–11960. [PubMed: 10508398]

[10]. Huppman P, Arlt T, Penzkofer H, Schmidt S, Bibikova M, Dohse B, Oesterhelt D, Wachvelt J, Zinth W. Kinetics, energetics, and electronic coupling of the primary electron transfer reactions in mutated reaction centers of *Blastochloris viridis*. Biophys. J 2002;82:3186–3197. [PubMed: 12023243]

[11]. Allen, JP.; Williams, JC. The influence of protein interactions on the properties of the bacteriochlorophyll dimer in reaction centers. In: Grimm, R.J.P. Bernhard; Rudiger, Wolfhart; Scheer, Hugo, editors. Chlorophylls and Bacteriochlorophylls: Biochemistry, Biophysics, Functions and Applications. Springer; 2006. p. 283-295.

[12]. Ermler U, Fritzsch G, Buchanan SK, Michel H. Structure of the photosynthetic reaction center from *Rhodobacter sphaeroides* at 2.65 Å resolution: cofactors and protein—cofactor interactions. Structure 1994;2:925–936. [PubMed: 7866744]

[13]. Bylina EJ, Youvan DC. Directed mutations affecting spectroscopic and electron transfer properties of the primary donor in the photosynthetic reaction center. Proc. Natl. Acad. Sci. U. S. A 1988;85:7226–7230. [PubMed: 16578836]

[14]. Bylina EJ, Kirmaier C, McDowell L, Holten D, Youvan DC. Influence of an aminoacid residue on the optical properties and electron transfer dynamics of a photosynthetic reaction center complex. Nature 1988;336:182–184.

[15]. Fajer J, Brune DC, Davis MS, Forman A, Spaulding LD. Primary charge separation in bacterial photosynthesis: oxidized chlorophylls and reduced pheophytin. Proc. Natl. Acad. Sci. U. S. A 1975;72:4956–4960. [PubMed: 174084]

[16]. Kirmaier C, Bylina EJ, Youvan DC, Holten D. Subpicosecond formation of the intradimer charge transfer state [BChlLP$^{+}$BPhMP$^{-}$] in reaction centers from the His$^{M200}$-Leu mutant of *Rhodobacter capsulatus*. Chem. Phys. Lett 1989;159:251–257.

[17]. Bylina EJ, Kolaczkowski SV, Norris JR, Youvan DC. EPR characterization of genetically modified reaction centers of *Rhodobacter capsulatus*. Biochemistry 1990;29:6203–6210. [PubMed: 2169865]

[18]. McDowell LM, Kirmaier C, Holten D. Temperature-independent electron transfer in *Rhodobacter capsulatus* wild-type and His$^{M200}$-Leu photosynthetic reaction centers. J. Phys. Chem 1991;95:3379–3383.

[19]. Palaniappan V, Bocian DF. Resonance Raman characterization of H(M200)L mutant reaction centers from *Rhodobacter capsulatus*. Effects of heterodimer formation on the structural and electronic properties of the bacteriochlorin cofactors. Biochemistry 1995;34:11106–11116. [PubMed: 7669768]

[20]. Kirmaier C, Bautista JA, Laible PD, Hanson DK, Holten D. Probing the contribution of electronic coupling to the directionality of electron transfer in photosynthetic reaction centers. J. Phys. Chem. B 2005;109:24160–24172. [PubMed: 16375408]

[21]. Allen JP, Artz K, Lin X, Williams JC, Ivancich A, Albouym D, Mattioli TA, Fetsch A, Kuhn M, Lubitz W. Effects of hydrogen bonding to a bacteriochlorophyll—bacteriopheophytin dimer in reaction centers from *Rhodobacter sphaeroides*. Biochemistry 1996;35:6612–6619. [PubMed: 8639609]

[22]. Brederode ME, Stokkum IHM, Katilius E, Mourik F, Jones MR, Grondelle R. Primary charge separation routes in the BChl:BPhe heterodimer reaction centers of *Rhodobacter sphaeroides*. Biochemistry 1999;38:7545–7555. [PubMed: 10360952]

[23]. Huber M, Isaacson RA, Abresch EC, Gaul D, Schenck CC, Feher G. Electronic structure of the oxidized primary electron donor of the HL(M202) and HL(L173) heterodimer mutants of the photosynthetic bacterium *Rhodobacter sphaeroides*: ENDOR on single crystals of reaction centers. Biochim. Biophys. Acta 1996;1273:108–128.

[24]. Nabedryk E, Schulz C, Muh F, Lubitz W, Breton J. Heterodimeric versus homodimeric structure of the primary electron donor in *Rhodobacter sphaeroides* reaction centers genetically modified at position M202. Photochem. Photobiol 2000;71:582–588. [PubMed: 10818789]

[25]. Camara-Artigas A, Magee C, Goetsch A, Allen JP. The structure of the heterodimer reaction center from *Rhodobacter sphaeroides* at 2.55 Å resolution. Photosynth. Res 2002;74:87–93. [PubMed: 16228547]

[26]. Niederman RA, Segen BJ, Gibson KD. Membranes of *Rhodopseudomonas spheroides*. I. Isolation and characterization of membrane fractions from extracts of aerobically and anaerobically grown cells. Arch. Biochem. Biophys 1972;152:547–560. [PubMed: 4539052]

[27]. Yen HC, Marrs B. Growth of *Rhodopseudomonas capsulata* under anaerobic dark conditions with dimethyl sulfoxide. Arch. Biochem. Biophys 1977;181:411–418. [PubMed: 900930]

[28]. Nitschke, W.; Dracheva, SM. Reaction center associated cytochromes. In: Blankenship, REMMT.; Bauer, CE., editors. Anoxygenic Photosynthetic Bacteria. Kluwer Academic Publishers; 1995. p. 775-805.

[29]. Matsuura K, Shimada K. Evolutionary relationships between reaction center complexes with and without cytochrome *c* subunits in purple bacteria. Proc. Int. Conf. Photosynth., 8th 1990;1:193–196.

[30]. Matsuura K. Comparative and evolutionary aspects of the photosynthetic electron transfer system of purple bacteria. J. Plant Res 1994;107:191–200.

[31]. Nagashima KVP, Hanada S, Hiraishi A, Shimada K, Matsuura K. Phylogenetic analysis of photosynthetic reaction centers of purple bacteria and green filamentous bacteria. Photosynthesis: from light to biosphere 1995;1:975–978.

[32]. Wachtveitl J, Farchaus JW, Mathis P, Oesterhelt D. Tyrosine 162 of the photosynthetic reaction center L-subunit plays a critical role in the cytochrome $c_2$ mediated rereduction of the photooxidized bacteriochlorophyll dimer in *Rhodobacter sphaeroides*. 2. Quantitative kinetic analysis. Biochemistry 1993;32:10894–10904. [PubMed: 8399239]

[33]. Axelrod HL, Abresch EC, Okamura MY, Yeh AP, Rees DC, Feher G. X-ray structure determination of the cytochrome $c_2$: reaction center electron transfer complex from *Rhodobacter sphaeroides*. J. Mol. Biol 2002;319:501–515. [PubMed: 12051924]

[34]. Lin X, Williams JC, Allen JP, Mathis P. Relationship between rate and free energy difference for electron transfer from cytochrome $c_2$ to the reaction center in *Rhodobacter sphaeroides*. Biochemistry 1994;33:13517–13523. [PubMed: 7947761]

[35]. Rautter J, Lendzian F, Schulz C, Fetsch A, Kuhn M, Lin X, Williams C, Allen JP, Lubitz W. ENDOR studies of the primary donor cation radical in mutant reaction centers of *Rhodobacter sphaeroides* with altered hydrogen-bond interactions. Biochemistry 1995;34:8130–8143. [PubMed: 7794927]

[36]. Rautter, J.; Lendzian, F.; Lin, X.; Williams, JC.; Allen, JP.; Lubitz, W.; Feher, G. Effect of orbital asymmetry in $P^+$ on electron transfer in reaction centers of *Rhodobacter sphaeroides*. In: Michel-Beyerle, M-E., editor. The Reaction Center of Photosynthetic Bacteria: Structure and Dynamics. Springer; Berlin: 1996. p. 37-50.

[37]. Adir N, Axelrod HL, Beroza P, Isaacson RA, Rongey SH, Okamura MY, Feher G. Co-crystallization and characterization of the photosynthetic reaction center—cytochrome $c_2$ complex from *Rhodobacter sphaeroides*. Biochemistry 1996;35:2535–2547. [PubMed: 8611557]

[38]. Nitschke W, Rutherford AW. Tetraheme cytochrome *c* subunit of *Rhodopseudomonas viridis* characterized by EPR. Biochemistry 1989;28:3161–3168.

[39]. Kaminskaya O, Bratt PJ, Evans MCW. EPR properties of the four hemes in the cytochrome subunit of reaction centers from *Rhodopseudomonas viridis*: characterization of the individual hemes. Chem. Phys 1995;194:335–348.

[40]. Dracheva SM, Drachev LA, Zaberezhnaya SM, Konstantinov AA, Semenov AY, Skulachev VP. Spectral, redox and kinetic characteristics of high-potential cytochrome *c* hemes in *Rhodopseudomonas viridis* reaction center. FEBS Lett 1986;205:41–46.

[41]. Nabedryk E, Berthomieu C, Vermeglio A, Breton J. Photooxidation of high-potential (c559, c556) and low-potential (c552) hemes in the cytochrome subunit of *Rhodopseudomonas viridis* reaction center. Characterization by FTIR spectroscopy. FEBS Lett 1991;293:53–58. [PubMed: 1660005]

[42]. Ortega JM, Mathis P. Electron transfer from the tetraheme cytochrome to the special pair in isolated reaction centers of *Rhodopseudomonas viridis*. Biochemistry 1993;32:1141–1151. [PubMed: 8381025]

[43]. Kaminskaya O, Konstantinov AA, Shuvalov VA. Low-temperature photooxidation of cytochrome *c* in reaction center complexes from *Rhodopseudomonas viridis*. Biochim. Biophys. Acta 1990;1016:153–164.

[44]. Frolov EN, Goldanskii VI, Birk A, Parak F. The influence of electrostatic interactions and intramolecular dynamics on electron transfer from the cytochrome subunit to the cation-radical of the bacteriochlorophyll dimer in reaction centers from *Rhodopseudomonas viridis*. Eur. Biophys. J 1996;24:433–438.

[45]. Ortega JM, Dohse B, Oesterhelt D, Mathis P. Very fast electron transfer from cytochrome to the bacterial photosynthetic reaction center at low temperature. FEBS Lett 1997;401:153–157. [PubMed: 9013877]

[46]. Prince RC, Leigh JS, Dutton PL. Thermodynamic properties of the reaction center of *Rhodopseudomonas viridis*. In vivo measurement of the reaction center bacteriochlorophyll-primary acceptor intermediary electron carrier. Biochim. Biophys. Acta, Bioenerg 1976;440:622–636.

[47]. Prince RC, Tiede DM, Thornber JP, Dutton PL. Spectroscopic properties of the intermediary electron carrier in the reaction center of *Rhodopseudomonas viridis*. Evidence for its interaction with the primary acceptor. Biochim. Biophys. Acta 1977;462:467–490. [PubMed: 22348]

[48]. Lang FS, Oesterhelt D. Microaerophilic growth and induction of the photosynthetic reaction center in *Rhodopseudomonas viridis*. J. Bacteriol 1989;171:2827–2834. [PubMed: 2651419]

[49]. Maki H, Matsuura K, Shimada K, Nagashima KVP. Chimeric photosynthetic reaction center complex of purple bacteria composed of the core subunits of *Rubrivivax gelatinosus* and the cytochrome subunit of *Blastochloris viridis*. J. Biol. Chem 2003;278:3921–3928. [PubMed: 12464624]

[50]. Alric J, Lavergne J, Rappaport F, Vermeglio A, Matsuura K, Shimada K, Nagashima KVP. Kinetic performance and energy profile in a roller coaster electron transfer chain: a study of modified tetraheme-reaction center constructs. J. Am. Chem. Soc 2006;128:4136–4145. [PubMed: 16551123]

[51]. Alric J, Cuni A, Maki H, Nagashima KVP, Vermeglio A, Rappaport F. Electrostatic interaction between redox cofactors in photosynthetic reaction centers. J. Biol. Chem 2004;279:47849–47855. [PubMed: 15347641]

[52]. Lancaster CR, Bibikova MV, Sabatino P, Oesterhelt D, Michel H. Structural basis of the drastically increased initial electron transfer rate in the reaction center from a *Rhodopseudomonas viridis* mutant described at 2.00 Å resolution. J. Biol. Chem 2000;275:39364–39368. [PubMed: 11005826]

[53]. Bylina EJ, Ohgi KA, Nute T, Cerniglia V, O'Neal S, Weaver P. A system for site-directed mutagenesis of the photosynthetic apparatus in *Blastochloris viridis*. Biotechnol. et alia 2002;9:1–23.www.et-al.com

[54]. Sambrook, J.; Fritsch, E.; Maniatis, T. Molecular Cloning: A Laboratory Manual. Vol. 2nd ed. Cold Spring Harbor Press; Cold Spring Harbor, NY: 1989.

[55]. Weyer KA, Lottspeich F, Gruenberg H, Lang F, Oesterhelt D, Michel H. Amino acid sequence of the cytochrome subunit of the photosynthetic reaction center from the purple bacterium *Rhodopseudomonas viridis*. EMBO J 1987;6:2197–2202. [PubMed: 16453786]

[56]. Weaver PF, Wall JD, Gest H. Characterization of *Rhodopseudomonas capsulata*. Arch. Microbiol 1975;105:207–216. [PubMed: 1103769]

[57]. Fritzsch G. Obtaining crystal structures from bacterial photosynthetic reaction centers. Methods Enzymol 1998;297:57–77.

[58]. Michel H. Three-dimensional crystals of a membrane protein complex. The photosynthetic reaction centre from *Rhodopseudomonas viridis*. J. Mol. Biol 1982;158:567–572. [PubMed: 7131557]

[59]. Li L, Mustafi D, Fu Q, Tereshko V, Chen DL, Tice JD, Ismagilov RF. Nanoliter microfluidic hybrid method for simultaneous screening and optimization validated with crystallization of membrane. Proc. Natl. Acad. Sci. U. S. A 2006;103:19243–19248. [PubMed: 17159147]

[60]. Otwinowski, Z.; Minor, W. Processing of X-ray diffraction data collected in oscillation mode. In: Caster, RMSCW., editor. Macromolecular Crystallography Pt A. Vol. 276. Academic Press Inc.; San Diego: 1997. p. 307-326.

[61]. Murshudov GN, Vagin AA, Dodson EJ. Refinement of macromolecular structures by the maximum-likelihood method. Acta Crystallogr., Sect. D Biol. Crystallogr 1997;53:240–255. [PubMed: 15299926]

[62]. Collaboration. The CCP4 suite: programs for protein crystallography. Acta Crystallogr., Sect. D Biol. Crystallogr 1994;50:760–763. [PubMed: 15299374]

[63]. Cambillau, C.; Roussel, A. Turbo Frodo. Vol. Version OpenGL 1. University Aix-Marseille II; Marseille, France: 1997.

[64]. Zwart P, Langer GG, Lamzin VS. Modelling bound ligands in protein crystal structures. Acta Crystallogr., Sect. D Biol. Crystallogr 2004;60:2230–2239. [PubMed: 15572776]

[65]. Emsley P, Cowtan K. Coot: model-building tools for molecular graphics. Acta Crystallogr., Sect. D Biol. Crystallogr 2004;60:2126–2132. [PubMed: 15572765]

[66]. Dutton PL. Redox potentiometry: determination of midpoint potentials of oxidation-reduction components of biological electron-transfer systems. Methods Enzymol 1978;54:411–435. [PubMed: 732578]

[67]. Tsujimura S, Kuriyama A, Fujieda N, Kano K, Ikeda T. Mediated spectro-electrochemical titration of proteins for redox potential measurements by a separator-less one-compartment bulk electrolysis method. Analyt. Biochem 2005;337:325–331. [PubMed: 15691513]

[68]. Hawkridge FM, Taniguchi I. The direct electron transfer reactions of cytochrome *c* at electrode surfaces. Comments Inorg. Chem 1995;17:163–187.

[69]. O'Reilly JE. Oxidation-reduction potential of the ferro-ferricyanide system in buffer solutions. Biochim. Biophys. Acta 1973;292:509–515. [PubMed: 4705442]

[70]. Schilt A, Cresswell AM. New colorimetric reagents for determination of trace amounts of oxidants and reductants. Talanta 1966;13:911–918. [PubMed: 18959953]

[71]. Nagarajan V, Parson WW, Davis D, Schenck CC. Kinetics and free energy gaps of electron-transfer reactions in *Rhodobacter sphaeroides* reaction centers. Biochemistry 1993;32:12324–12336. [PubMed: 8241119]

[72]. Arnoux B, Reiss-Husson F. Pigment—protein interactions in *Rhodobacter sphaeroides* Y photochemical reaction center: comparison with other reaction center structures. Eur. Biophys. J 1996;24:233–242.

[73]. Dohse B, Mathis P, Wachtveitl J, Laussermair E, Iwata S, Michel H, Oesterhelt D. Electron transfer from the tetraheme cytochrome to the special pair in the *Rhodopseudomonas viridis* reaction center: effect of mutations of tyrosine L162. Biochemistry 1995;34:11335–11343. [PubMed: 7547861]

[74]. Arlt T, Bibikova M, Penzkofer H, Oesterhelt D, Zinth W. Strong acceleration of primary photosynthetic electron transfer in a mutated reaction center of *Rhodopseudomonas viridis*. J. Phys. Chem 1996:100.

[75]. King BA, de Winter A, McAnaney TB, Boxer SG. Excited state energy transfer pathways in photosynthetic reaction centers. 4. Asymmetric energy transfer in the heterodimer mutant. J. Phys. Chem. B 2001;105:1856–1862.

[76]. Raibekas AA, Massey V. Glycerol-assisted restorative adjustment of flavoenzyme conformation perturbed by site-directed mutagenesis. J. Biol. Chem 1997;272:22248–22252. [PubMed: 9268372]

[77]. Roberge M, Shareck F, Morosoli R, Kluepfel D, Dupont C. Site-directed mutagenesis study of a conserved residue in family 10 glycanases: histidine 86 of xylanase A from *Streptomyces lividans*. Protein Eng 1998;11:399–404. [PubMed: 9681873]

[78]. Thomas A, Meurisse R, Brasseur R. Aromatic side-chain interactions in proteins. II. Near- and far-sequence Phe-X pairs. Proteins Struct. Funct. Genet 2002;48:635–644. [PubMed: 12211031]

[79]. Meurisse R, Brasseur R, Thomas A. Aromatic side-chain interactions in proteins. Near- and far-sequence His-X pairs. Biochim. Biophys. Acta 2003;1649:85–96. [PubMed: 12818194]

[80]. Thomas A, Meurisse R, Charloteaux B, Brasseur R. Aromatic side-chain interactions in proteins. I. Main structural features. Proteins Struct. Funct. Genet 2002;48:628–634. [PubMed: 12211030]

[81]. Brinda KV, Vishveshwara S. A network representation of protein structures: implications for protein stability. Biophys. J 2005;89:4159–4170. [PubMed: 16150969]

[82]. Allen JP, Williams JC, Feher G, Yeates TO, Komiya H, Rees DC. Structure of the reaction center from *Rhodobacter sphaeroides* R-26: the protein subunits. Proc. Natl. Acad. Sci. U. S. A 1987;84:6162–6166. [PubMed: 2819866]

[83]. Cartling B. A mechanism of temperature dependent electron transfer reactions in biological systems. J. Chem. Phys 1991;95:317–322.

[84]. Aquino AJA, Beroza P, Reagan J, Onuchic JN. Estimating the effect of protein dynamics on electron transfer to the special pair in the photosynthetic reaction center. Chem. Phys. Lett 1997;275:181–187.

[85]. Ortega JM, Dohse B, Oesterhelt D, Mathis P. Low-temperature electron transfer from cytochrome to the special pair in *Rhodopseudomonas viridis*: role of the L162 residue. Biophys. J 1998;74:1135–1148. [PubMed: 9512015]

[86]. Farchaus JW, Wachtveitl J, Mathis P, Oesterhelt D. Tyrosine 162 of the photosynthetic reaction center L-subunit plays a critical role in the cytochrome $c_2$ mediated rereduction of the photooxidized bacteriochlorophyll dimer in *Rhodobacter sphaeroides*. 1. Site-directed mutagenesis and initial characterization. Biochemistry 1993;32:10885–10893. [PubMed: 8399238]

[87]. Gong X-M, Paddock ML, Okamura MY. Interactions between cytochrome $c_2$ and photosynthetic reaction center from *Rhodobacter sphaeroides*: changes in binding affinity and electron transfer

rate due to mutation of interfacial hydrophobic residues are strongly correlated. Biochemistry 2003;42:14492–14500. [PubMed: 14661961]

[88]. Axelrod HL, Okamura MY. The structure and function of the cytochrome $c_2$: reaction center electron transfer complex from *Rhodobacter sphaeroides*. Photosynth. Res 2005;85:101–114. [PubMed: 15977062]

[89]. Davis D, Dong A, Caughey WS, Schenck CC. Energetics of the oxidized primary donor in wild type and hetero-dimer mutant reaction center. Biophys. J 1992;61:A153.(abstr)

[90]. Lathrop EJP, Friesner RA. Simulation of optical spectra from the reaction center of *Rhodobacter sphaeroides*. Effects of an internal charge-separated state of the special pair. J. Phys. Chem 1994;98:3056–3066.

[91]. Plato M, Lendzian F, Lubitz W, Moebius K. Molecular orbital study of electronic asymmetry in primary donors of bacterial reaction centers. NATO ASI Ser., Ser. A: Life Sci 1992;237:109–118.

[92]. Huber M. On the electronic structure of primary electron donor in bacterial photosynthesis — the bacteriochlorophyll dimer as viewed by EPR/ENDOR methods. Photosynth. Res 1997;52:21–26.

[93]. Lin X, Murchison HA, Nagarajan V, Parson WW, Allen JP, Williams JC. Specific alteration of the oxidation potential of the electron donor in reaction centers from *Rhodobacter sphaeroides*. Proc. Natl. Acad. Sci. U. S. A 1994;91:10265–10269. [PubMed: 7937938]

[94]. Laporte LL, Palaniappan V, Kirmaier C, Davis DG, Schenck CC, Holten D, Bocian DF. Influence of electronic asymmetry on the spectroscopic and photodynamic properties of the primary electron donor in the photosynthetic reaction center. J. Phys. Chem 1996;100:17696–17707.

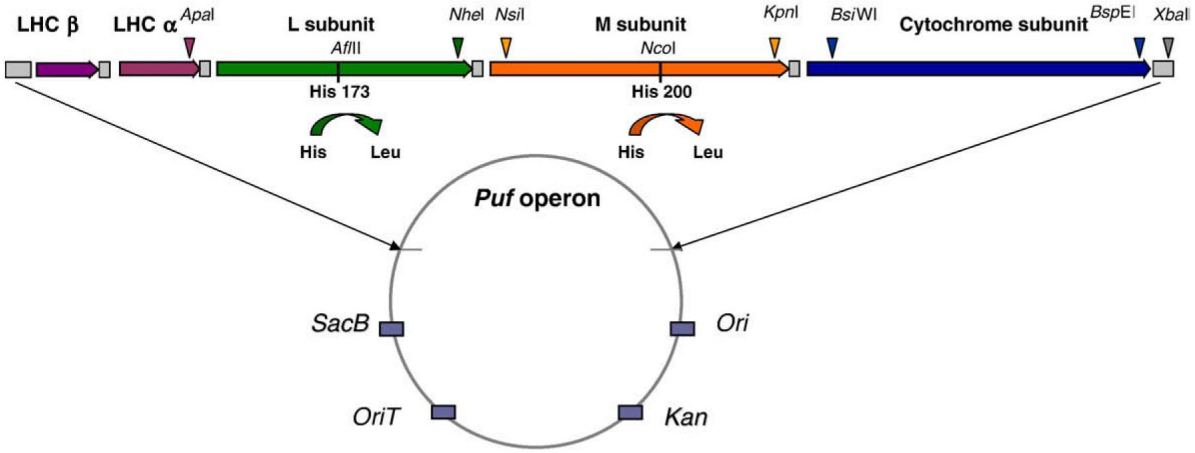


**Fig. 1.**

Complementing plasmid containing *B. viridis* DSM-133 *puf* operon structural genes. Unique restriction sites introduced in the *puf* operon to facilitate cloning and mutagenesis are shown. *Ori*, *Kan*, *OriT*, *SacB* represent the interposons containing an origin of replication, kanamicyn resistance gene, origin of transfer and counterselectable gene.

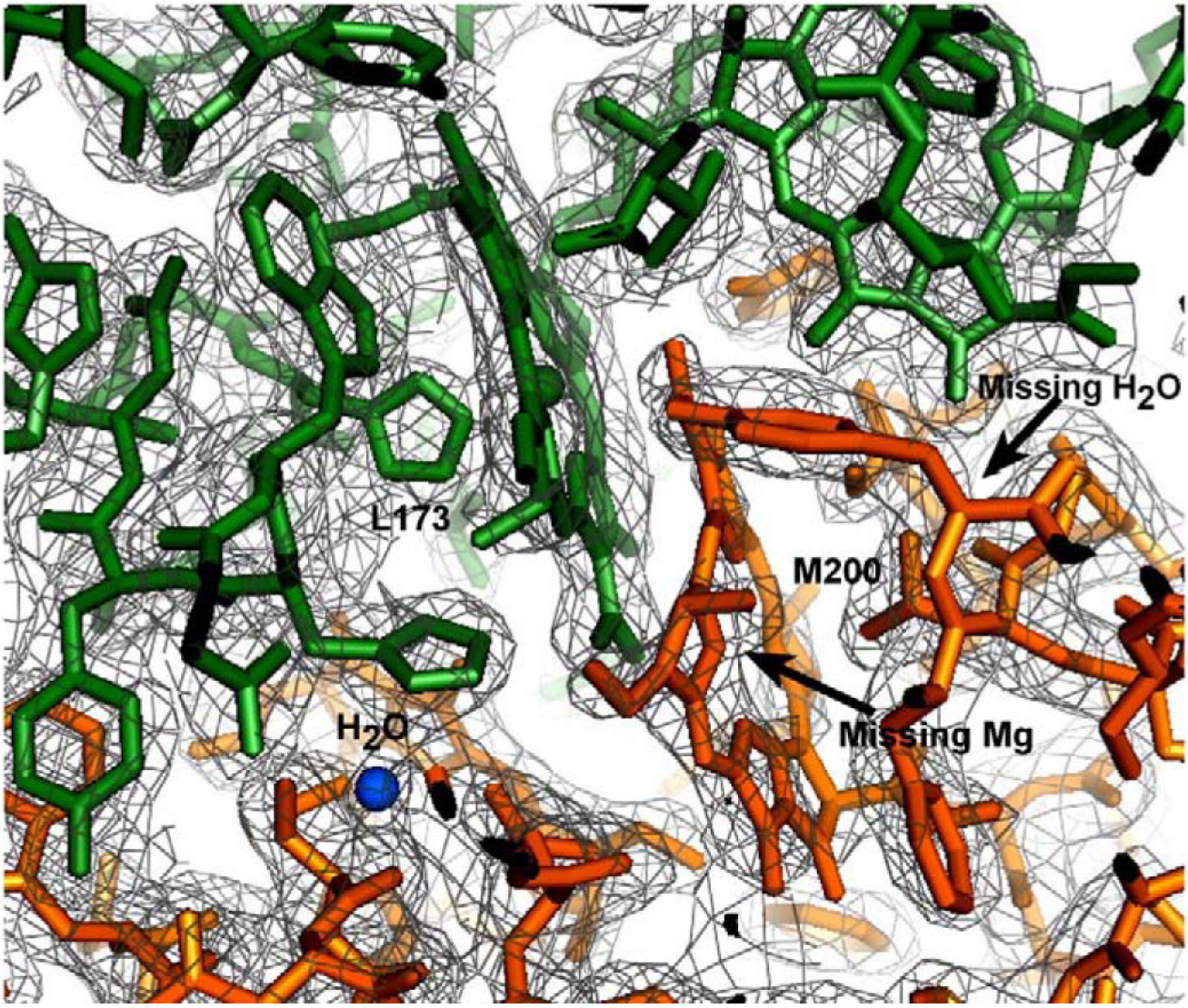


**Fig. 2.**

Electron-density map calculated between 20 and 2.5 Å resolution within 10 Å×10 Å×10 Å box around heterodimer primary donor in M mutant. The map is contoured at 1.0 σ. Note the presence of Mg in DL (middle of the left side of image) and its absence in DM, next to leucine. Aminoacids and cofactors associated with L side colored in green, with M side, — in orange.

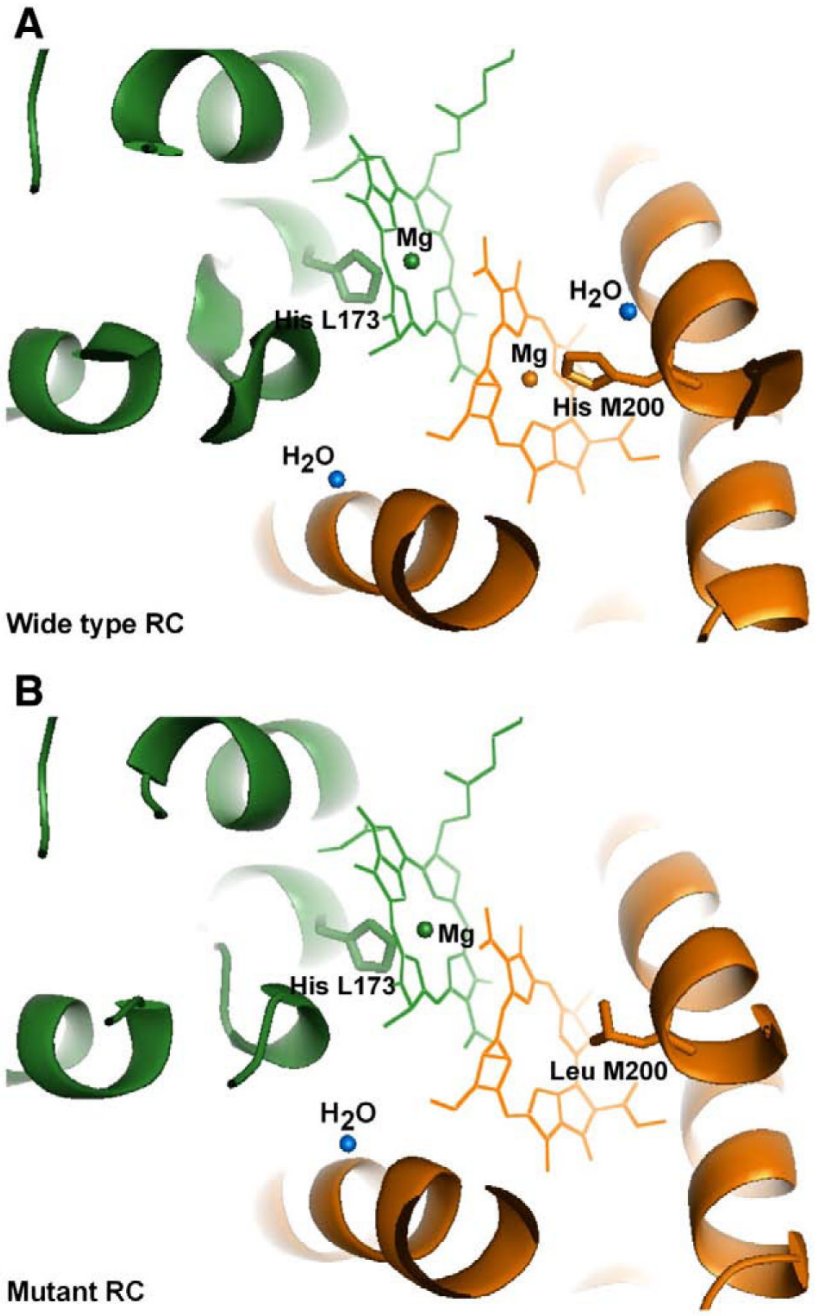


**Fig. 3.**
Reaction center structure in vicinity of primary donor. A — wild type. B — M-heterodimer mutant. Colors: green —L subunit, orange — M subunit.

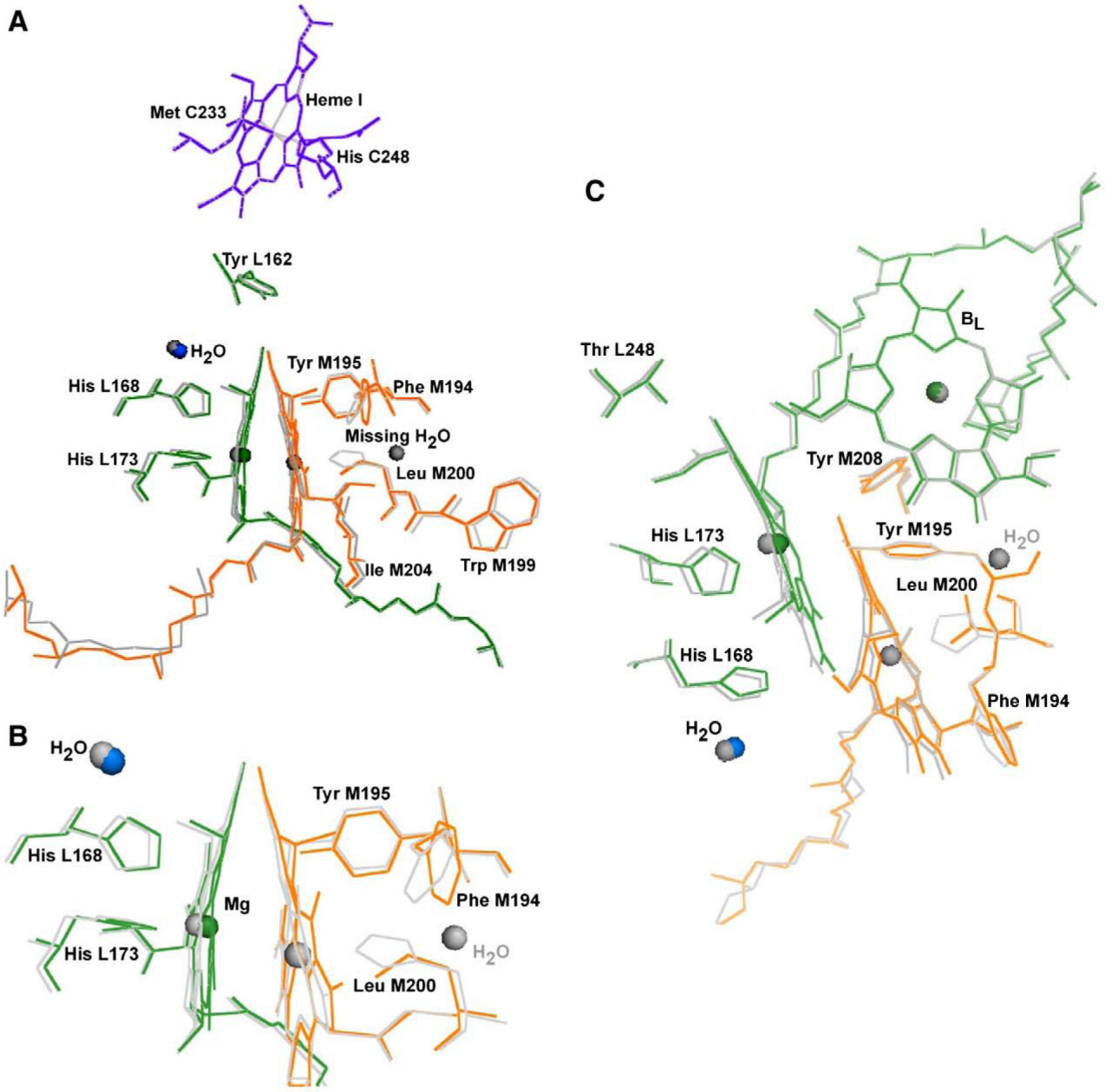


**Fig. 4.**

Superposition of wild type and M-heterodimer structures in vicinity of primary donor highlighting structural differences in positions of porphyrin molecules and ligands. Surrounding amino acids residues omitted for clarity. Colors used: grey for wild type, green for aminoacids and cofactors corresponding to L subunit, orange — to M subunit, purple — to heme 1 and its ligands. A — a view perpendicular to the two-fold symmetry axis of the primary donor, B — an expanded version of region (primary donor is orientated approximately along the two-fold symmetry axis), C — primary donor and accessory bacteriochlorophyll, a view parallel to the symmetry axis directed from the region of overlapping rings with 45° tilt.

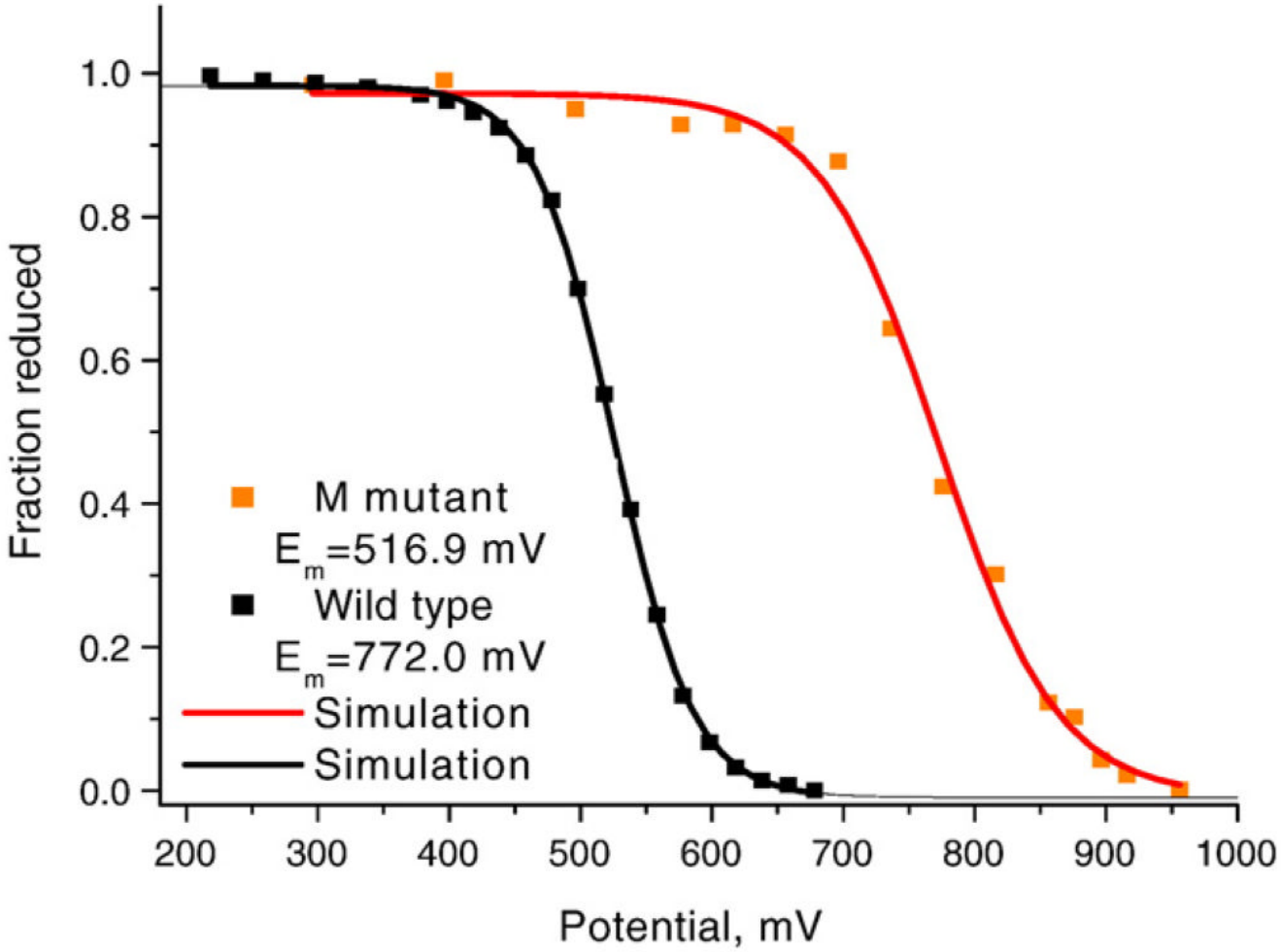


**Fig. 5.**
Spectropotentiometric titration of the primary donor in reaction centers isolated from wild type and M mutant. Potentials represented *vs*. SHE. The extent of dimmer reduction determined by monitoring the alteration of primary donor optical absorption in response to applied potential.

**Table 1**

Diffraction data collection and refinement statistics.

| | M mutant | Wild type |
|---|---|---|
| Data processing | | |
| Space group | $P4_32_12$ | $P4_32_12$ |
| Unit-cell dimensions a, b, c, Å | 220.1, 220.1, 112.7 | 220.4, 220.4, 113.0 |
| Diffraction resolution, Å | 50–2.50 (2.59–2.50)[a] | 50–1.96 (2.0–1.96) |
| Completeness, % | 99.2 (96.1) | 94.5 (67.4) |
| $R_{merge}$ | 0.137 (0.709) | 0.082 (0.48) |
| Redundancy | 7.1 (6.2) | 5.9 (4.1) |
| Refinement | | |
| $R_{work}/R_{free}$ | 0.173/0.204 | 0.172/0.186 |
| Number of atoms | | |
| Protein | 9296 | 9293 |
| Cofactors | 795 | 790 |
| Fe/Mg/$SO_4$ ions | 5/3/13 | 5/4/13 |
| Number of water molecules | 730 | 771 |
| Average B-factors, $Å^2$ | | |
| Protein atoms | 32.207 | 24.5 |
| Cofactors | 35.9 | 27.1 |
| Fe/Mg/$SO_4$ ions | 26.4/24.8/36.5 | 20.1/15.9/43.4 |
| Water molecules | 38.5 | 33.1 |
| Validation | | |
| Coordinate error, A° | 0.214 | 0.099 |
| RMS deviations from ideal values | | |
| Bond lengths, Å | 0.014 | 0.008 |
| Bond angles, ° | 1.487 | 1.330 |

[a] Values in parentheses are for the highest resolution shell.